The Impact of Dilution Air Strategy on n-heptane Turbulent Swirl Spray Flames

Abdallah Abu Saleh*, Kevin J. Hughes, Ruoyang Yuan

School of Mechanical, Aerospace and Civil Engineering, University of Sheffield, South Yorkshire, S10 2TN, United Kingdom

*Corresponding author. E-mail: a.abu.saleh@sheffield.ac.uk

Abstract

This paper investigates the impact of dilution air addition on the stability and flame structure of n-heptane turbulent swirl spray flames. Particle Image Velocimetry (PIV) was used to study the flow fields with and without dilution air. OH Planar Laser Induced Fluorescence (OH-PLIF) measurements were utilized to assess the impact of dilution air addition on flame structure, local extinction, and lift-off. Experimental results were collected at different flow conditions including quenching point (global blow-off), near blow-off, and stable conditions. 1D non-premixed laminar counter-flow flame simulations were also conducted to gain preliminary understanding of the flame structure behaviour and temperature when adding more air with hot products. The numerical results showed that adding 10% more air on the oxidiser side increased the peak values of the temperature, heat release rate (HRR) and OH mole fraction, with the maximum flame temperature rising by approximately 3.9%. The flame's stability limit increased when adding dilution air, and a 2% addition made the flame persist longer. The flame restabilized with the addition of 5% dilution air at the blow-off co-flow conditions of the non-diluted flames. OH* chemiluminescence results showed that the addition of dilution air up to 10% of the co-flow increased the heat release rate by as much as 247%, indicating a strong enhancement in flame intensity and reaction zone activity. The addition of dilution showed the droplets to spread more widely into the inner recirculation zone (IRZ). PIV

showed a clear displacement of the vortex inwards and upwards when adding dilution air, with increased turbulence intensity aligned with shear layers. Without dilution air, the OH flame sheet appeared continuous, while with dilution air, it appeared to be wrinkled, cloud-shaped, and distributed. Statistical analysis of the OH-PLIF results showed that adding 5% dilution air increased local extinction events by up to 7.5%, primarily due to the intense aerodynamic strain imposed on the flame front under highly turbulent conditions. OH-PLIF results showed that the addition of dilution air increases the relative OH intensity in the outer flame branch (OFB) at the same horizontal plane downstream. The novel findings on extended operation condition effect by adding dilution air provide the first evidence of enhanced flame stabilization towards lean combustion strategy.

Keywords: Dilution air; Spray flame; PLIF; Local extinction; Lift-off

1. Introduction

Flame stabilization is fundamentally crucial in the effective operation and design of combustion systems, particularly aero-engines. The main aim of flame stabilization is to prevent blow-off leading to flameout. Achieving the stability feature enhances the flexibility to operate in low emission mode over a wide-ranging load [1]. Different techniques have been developed to help with flame stabilization, depending on the engine type, such as swirl stabilization and pilot flames. Among these, the bluff-body is widely used because of its simplicity and effectiveness in generating a stable recirculation zone that anchors the flame [2]. The swirl stabilized combustion concept, which provides advantages such as better turbulent mixing and flame stabilization, has been widely used in aero-engines [3]. Swirling flows generate an inner recirculation zone (IRZ) within the flame creating an ideal condition for the hot, recirculated products to maintain the ignition process of newly injected reactants into the combustor [4]. The strategy of a secondary injection of dilution air downstream of the combustion chamber, also known as the Rich-Burn, Quick-Mix, Lean-Burn (RQL) combustor, of gas turbine engines was introduced in 1980 primarily to reduce the NOx emissions [5]. For optimal operation, modern burners use the bluff-body swirling flames along with the dilution air strategy [6].

While the current study investigates a single liquid fuel with secondary air injection, the downstream air injection methodology is transferable to dual-fuel and partially premixed combustion strategies, where staged injection influences flame structure and emissions formation. Several studies have investigated the impact of dual-fuel and partially premixed combustion strategies on pollutant formation, flame structure, and ignition behaviour under different conditions [7,8]. Liu et al [7] compared partially premixed combustion and reactivity controlled compression ignition in an optical engine using different optical diagnostics to study fuel stratification, ignition and flame development. They reported that the degree of fuel

stratification, controlled via different injection strategies, modulated the balance between these two combustion modes. More recently, from their optical diagnostics and chemical kinetic analysis partially premixed combustion of methanol with various cetane improvers, Liu et al. [8] reported that the ignition and heat release characteristics were greatly affected by the reactive environment created by fuel additives.

The dilution air strategy reduces the amount of NO_x emissions significantly as its addition results in a leaner combustion at lower combustion temperatures. However, lean combustion is associated with an elevated risk of extinction, which can ultimately lead to a global blow-off event [9]. Wang et al. [10] studied the impact of secondary (dilution) air distribution on combustion and NOx emissions in a swirl down-fired boiler. They found that as the dilution air level increased, NOx emissions decreased continuously, and the optimum air-staging condition reduced NOx emissions by approximately 46% without compromising the thermal efficiency of the burner. Kikuchi et al. [11] showed that two-stage combustion with parallel independent air jets can reduce NOx production in ammonia/ natural gas flames. The NOx reduction was attributed to the formation of a fuel-rich zone downstream of the burner, followed by lean combustion of the unburned portion with secondary air. Trivanovic and Pratsinis [12] studied the trade-off between soot and NO emissions during enclosed spray combustion of Jet A1 fuel. They reported that the location of dilution air injection affected both pollutants; air injected closer to the burner resulted in the greatest reduction in soot emissions but produced higher NO levels because of the elevated post-injection temperatures. They concluded that an injection position of 30 cm downstream provided the best trade-off between soot and NO emissions.

Many studies investigated the impact of different operating parameters including the injection of dilution air on soot emission, oxidation, and particle size distribution of swirl-stabilized flames [6,13–17]. Geigle et al. [15,16] studied the effect of dilution air at a fixed

location on soot emission, oxidation and polycyclic aromatic hydrocarbons (PAH) of ethylene air swirl-stabilized flames using laser-induced incandescence and PAH-LIF. They observed that the addition of dilution air had an impact on the location of soot areas as well as OH distributions in the flames. In addition, they investigated the relationship between soot and OH distributions after the dilution air introduction. Stöhr et al [17] observed that soot accumulates in the rich pockets depending on their residence times, while soot oxidation takes place in the lean zones containing OH. Their findings imply that a suitable modification of dilution air injection creating adequate recirculation of lean burnt gas may further limit the formation of soot. El Helou et al. [13] investigated the influence on soot formation and oxidation by varying the locations and amount of dilution air in C_2H_4 air (gaseous fuel) flames. Their outcomes revealed that dilution air resulted in a faster mixing, and smaller lengths of fuel penetration. In addition, their findings demonstrated that the quantity and location of injected dilution air affect the soot production. De Falco et al. [14] further investigated the soot formation in a non-premixed ethylene air flames but focusing more on their particle size distribution. El Helou et al. [6] carried out a comparison on the soot formation of synthetic kerosene and conventional fossil liquid fuels in a swirl spray flames along with air dilution injection. Their results showed that the distribution of SVFs is dependent on the quantity of dilution air.

The fuel properties (e.g., volatility) and swirl-induced recirculation zone both affect flame stabilization mechanisms and lean blow-off (LBO) limits. Few studies investigated the LBO conditions of different fuels in swirl spray burners [3,18–22]. Farag et al. [18] evaluated the effect of fuel volatility on LBO by using four different fuels, heavy oil was the least volatile and gasoline was the most. According to their findings, the rate of the air stream near the LBO limit increases as the fuel volatility increases, improving combustion stability. Although Yuan et al. [19] used a variety of high and low volatility fuels, their results addressing the effect of fuel volatility on flame stability were in good accord with those of Farag et al. [18]. Numerous

studies have investigated the fuel structure of n-heptane both numerically and experimentally in swirl spray flames, the appearance being of a dual body with a V shape that has inner and exterior sections [19]. The flame steadily shrinks and both sections get closer to the bluff-body as it approaches the blow-off condition by increasing air stream speed. Davide et al. [20] studied the blow-off behaviour of an n-heptane spray flame. They discovered that the loss of flame stability causes the velocity to become independent of fuel flow rate at blow-off. The height of the flame decreased and remained affixed to the bluff-body as the LBO condition approached. Also, it was discovered that the chemiluminescence of OH* was lower in the inner flame zone and higher at the outer flame zone. They observed a continuous layer of OH in their spray flame structure, which pointed to local blow-off activity. Pathania et al. [21] investigated the LBO conditions of fully premixed, swirl-stabilized methane and kerosene flames. They found that the kerosene flame exhibited approximately 1.5 times longer blow-off duration and better stability than the methane flame due re-ignition events and the presence of low-temperature reactions within the central recirculation zone. Zhang et al. [22] investigated the flame dynamics of swirl-stabilized kerosene spray combustion at stable and near LBO conditions. Their high-speed OH* chemiluminescence and POD analysis showed that as the flame approached near LBO condition, the dominant dynamic mode transitioned from circumferential rotation to axial oscillation, accompanied by flame shedding and stronger fluctuations. Their results also showed that the swirl intensity strongly influences flame oscillation behavior, with a lower swirl number reducing flame fluctuation near LBO.

Although many studies have investigated the n-heptane combustion characteristics in swirl spray flames, none have examined its combustion behaviour and stability under the influence of a dilution air strategy. This study addresses that gap by investigating the effects of dilution air on flame structure and stabilization using advanced optical diagnostics, including Fuel-PLIF, OH-PLIF, and PIV. The understanding of the flame stabilities with dilution air will help

engine manufactures design next-generation aero engines with improved fuel efficiency and extended operation conditions.

2. Methodology

2.1 Numerical study

1D non-premixed laminar counter flow flame simulations were carried out to gain preliminary understanding of the flame structure behaviour and temperature when adding more air with hot products. The San Diego chemical kinetic mechanism [23] was used to conduct the simulations of 1D n-heptane non-premixed laminar diffusion flame simulations with the COSILAB package [24]. The mixing conditions of the fuel, air and hot products used in the 1D simulations are shown in Table 1. Two pure n-heptane flame conditions were investigated; one case (#1) with an oxidiser of hot combustion products, which can be considered as a close representation of the interaction in the shear layer (reaction zone area) of the swirl spray flame (without dilution air). The second case (#2) is with an oxidiser of 10% of air and 90% of hot combustion products (which has the same composition as in case (#1)), representing the impact of dilution air. The composition of the hot combustion products used in this study were considered based on laminar premixed flame calculations suggested by Sidey and Mastorakos [25]. The strain rate was varied between 1000 to 2000 s^{-1} to understand better the flame structure at conditions away and close to extinction. The simulated flame cases were set to a fixed fuel inlet temperature of 298 K, whereas the oxidiser inlet temperature was fixed at 1838 K for all cases. Swirling flows generate an inner recirculation zone (IRZ) within the flame, creating an ideal condition for the hot, recirculated products to keep the newly injected reactants into the combustor constantly ignited. Therefore, the high inlet temperature set for the oxidiser and the introduction of hot products in the oxidiser stream provide a closer representation of the hot products generated in the swirl spray flames.

Table 1 Molar concentrations of the oxidiser stream for the 1D simulations of pure n-heptane counter flow flames.

Case	X_{O_2}	X_{N_2}	X_{H_2O}	X_{OH}	X_{CO_2}	X_{NO}
#1	0.06	0.729258	0.14	7.3×10^{-4}	0.07	1.2×10^{-5}
#2	0.075	0.7353322	0.126	7.6×10^{-4}	0.063	1.1×10^{-5}

2.2 Burner and experimental setup

A bluff-body swirl spray burner was used to investigate different flame conditions with and without dilution air. A similar burner was used in previous studies by Abu Saleh et al. [26,27], however in this study two separate tubes were inserted through the top section of the confined chamber of the burner to deliver the dilution air. A schematic of the bluff-body swirl spray burner is shown in Fig. 1. The two dilution air ports were placed at a height above the burner surface, each at a corner facing the other diagonally. The hole at the end of each dilution air port has a size of 1.5 mm diameter. A solid-cone fuel atomizer is placed between the bluff-body, providing a cone-like shape of fuel spray atomisation with an angle of 60°. The co-flow air travelled through a six-bladed swirl (60° vane angle) before entering the confined combustion chamber. An SXC 4 air compressor supplied both the dilution air and the co-flow air (dried, oil and particulate filtered). Separate calibrated mass flow controllers were used to control the dilution air and co-flow air streams. A calibrated Coriolis flow controller (CODA) was used to control the flow of n-heptane fuel.

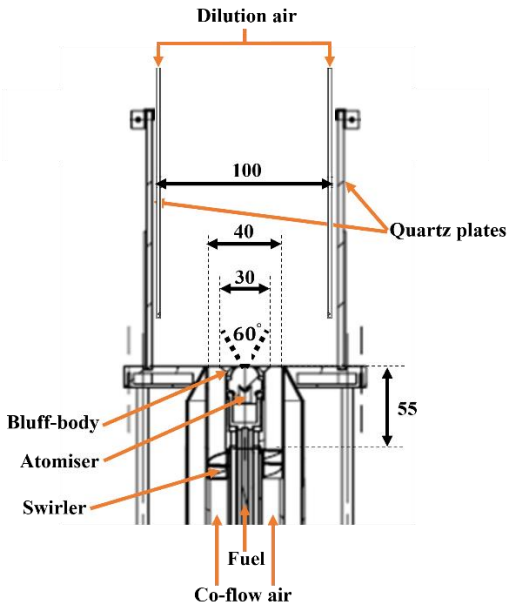

Fig. 1 Schematic of the bluff-body swirl spray burner [26] and dilution air tubes. Dimensions are all in mm.

2.3 Flow conditions

In this work, liquid fuel of pure n-heptane was tested in a bluff-body swirl spray burner with and without dilution air to study the impact of dilution air on flame stability, HRR, and reaction zone. Data were collected at the quenching point (global blow-off), near blow-off, and stable conditions. The global blow-off point was identified for each condition to help determine the near blow-off condition. This was done by gradually increasing the air flow rate in steps of around 5% every 1 minute until blow-off occurred. The air flow rate for the near blow-off condition was selected at between 9-15% lower than the air flow rate of the global blow-off (quenching) point. The air flow rate for the near blow-off condition was not selected based on a specific percentage difference from the air flow rate of the global blow-off. Instead, it was selected at that closest rate to the air flow rate of the global blow-off, in which the flame can sustain for at least 4 minutes.

Dilution air was added with 5% of the annular air flow rate to study its impact on various characteristics. For example, if 790 Standard Liter per Minute (SLPM) is the annular air flow

rate, the dilution air is 39.5 SLPM (5%). The impact of dilution air with different percentages including 2%, 5%, and 10% was also tested on one condition.

The flow conditions and fuel properties are shown in Table 2. For the first letter of the case name, Q denotes to the quenching (global blow-off) conditions, N as conditions nearer to blow-off, and S as stable conditions. For the second letter of the case name, N denotes to the cases with no air dilution, and D as conditions with air dilution. For the third letter of the case name, L denotes to the cases with low fuel flow rate of 630 g/h, whereas H denotes to the cases with higher fuel flow rate of 700 g/h.

Table 2 Turbulent swirl spray flames with and without Dilution Air strategy conditions.

Case Name	Fuel flow rate (g/h)	Annular Air flow rate (SLPM)	Dilution Air flow rate (SLPM)	Global equivalence ratio ϕ	Power (kW)	Fuel Reynolds No. Re_f	Air Reynolds No. Re_a	Fuel Weber No. We_f	Air Weber No. We_a
QN_L	630	790	0	0.167	8.4	2.62×10^3	1.57×10^4	3.66×10^2	3.01
QD_L		790	39.5 (5%)	0.162			1.65×10^4		3.47
NN_L		700	0	0.192			1.39×10^4		2.09
ND_L		700	35 (5%)	0.183			1.46×10^4		2.43
SN_L		600	0	0.223			1.19×10^4		1.26
SD_L		600	30 (5%)	0.213			1.25×10^4		1.49
QN_H	700	880	0	0.169	9.36	2.92×10^3	1.75×10^4	4.52×10^2	3.75
QD_H		880	44 (5%)	0.161			1.84×10^4		4.32
SN_H		790	0	0.188			1.57×10^4		2.71
SD1_H		790	15.8 (2%)	0.185			1.60×10^4		2.88
SD2_H		790	39.5 (5%)	0.179			1.65×10^4		3.14
SD3_H		790	79 (10%)	0.171			1.73×10^4		3.61

2.4 PIV

Cold flow (i.e. non-reacting flow) velocity field measurements were obtained for all conditions via Particle Image Velocimetry (PIV) measurements at 14.5 Hz. These were performed using a Quantel Evergreen EVG00200 Nd:YAG laser (532 nm) system, generating two laser pulses with a time-step of 5.5 μs. The laser energy generated from each pulse was about 28 mJ, and was passed through a set of optics to form an expanded laser sheet aligned to the centre of the swirl spray burner. A TSI six-jet atomizer fed with olive oil and compressed air generated the seeding particles that traveled through the annular airflow. The seeding particles signal were

detected by an intensified CCD camera (TSI) coupled with a narrow bandpass filter centred at 532 nm and a full width-half maximum (FWHM) of 10 nm. The resolution achieved for the PIV measurements was 0.48 mm/pixel. The MATLAB based open-source PIV software (PIVlab 3.06) [28] was used to process the PIV images. The background noise was reduced by subtracting the mean background from the raw images. A multi-pass cross-correlation technique was employed in the PIV algorithm with an interrogation region overlapping by 50% to determine the displacements from an image pair. The interrogation window area size (pixel) and the step size (pixel) of the Multipass FFT window PIV algorithm (three passes) were 128x64, 64x32, and 32x16 pixels.

The turbulent kinetic energy (*TKE*) of all conditions were estimated using the root mean square (RMS) velocity components (2D velocity fields) [29]:

$$TKE = \frac{1}{2}(u'^2 + v'^2) \quad (1)$$

Where u' and v' correspond to the radial and axial RMS velocity fluctuation components, respectively. In the current *TKE* calculations, it is assumed that the radial fluctuations are equivalent to the out of plane velocity fluctuations since only 2D velocity fields are measured [30]. The cold flow PIV results that correspond to the SN_H, SD1_H, SD2_H, and SD3_H conditions will only be shown in the results and discussions section, the remaining results are attached to the appendix.

2.5 Chemiluminescence

OH* chemiluminescence imaging was used as a measure of heat release for the QN_L, QD_L, NN_L, ND_L, SN_L, and SD_L conditions. The chemiluminescence images were captured at 10 Hz and 200 frames were collected for each flame condition. An intensified CCD camera (M-lite from LaVision) coupled with a narrow bandpass UV filter centred at 310 nm and a FWHM of 10 nm was used as the detection system. The camera exposure duration and

intensifier gain were set to 20000 ns and 65, respectively. The background noise was reduced by background subtraction and the use of 2-D median filtering.

The Inverse Abel Transform (IAT) mathematical approach (onion-peeling) was employed on the mean chemiluminescence images to reconstruct line-of-sight chemiluminescence data and provide 2D chemiluminescence images, assuming that the chemiluminescence were axisymmetric. Due to the turbulent nature of the flame, the IAT was only applied to the mean images. However, the mean chemiluminescence images of the flame are not always axisymmetric, hence only one-half of the mean image was chosen for the IAT to reconstruct an axisymmetric image [31].

2.6 PLIF

The OH-PLIF diagnostic technique was applied on flame conditions to investigate the impact of dilution air addition on flame sheet characteristics. OH-PLIF images were also used to study local extinction and lift-off characteristics in different flame conditions. An Nd:YAG pumped dye laser was used to generate a laser light sheet at approximately 283 nm wavelength that passed through the centre of the flame to excite the Q1(6) rotational transition (282.927 nm) in the $A^2\sum - X^2\prod(1,0)$ band.. The detection system comprised of a 308 nm narrow bandpass filter mounted on a LaVision camera (ICCD) perpendicular to the light sheet.

Background noise was removed by background subtraction and the application of the 2-D median filtering technique. Background images B(Q) were collected for each condition at an off-resonance laser wavelength of 282.800 nm. The background images provided the opportunity to gain insights into the impact of dilution air addition on fuel spray atomisation through the fuel fluorescence signal (fuel-PLIF).

Lift-off height was measured as the axial distance above the burner surface and the closest bottom edge of the flame sheet in the outer recirculation zone (ORZ), after that, The probability

density function (PDF) of lift-off heights was then plotted. The PDF of local extinctions were processed in a similar way described by Abu Saleh et al. [26].

3. Results and discussions

3.1 Laminar counter flow flames

The laminar counter flow flame simulation results of temperature, OH mole fraction, and heat release rate for pure n-heptane flame (#1 and #2 flame conditions) at strain rates of 1000 s^{-1} and 2000 s^{-1} are shown in Fig. 2. The addition of 10% more air (#2 flame condition) on the oxidiser side increased the peak values of the temperature and HRR. Fig. 2 shows that introducing dilution air increases the maximum flame temperature by approximately 3.8% and 3.9% at strain rates of 1000 s^{-1} and 2000 s^{-1}, respectively. The increased air in the oxidiser side makes the fuel burn more completely because more O_2 becomes available in the mixture. Consequently, the flame combustion generates more heat, increasing the flame's temperature, as shown in Fig. 2. Adding 10% more air also increased the OH mole fraction. Increasing the OH mole fraction promotes more combustion reactions and increases the flame's temperature. Therefore, the flame stability can be enhanced by the increase in the concentration of OH. As expected, the increase in the strain rate from 1000 s^{-1} to 2000 s^{-1} decreased the peak values of temperature, OH mole fraction, and heat release rate. However, the increase in strain rate decreased the flame temperature by about 1.6% for #1 and 1.5% for #2. Therefore, it is expected that the case with an oxidiser of 10% more air will sustain longer.

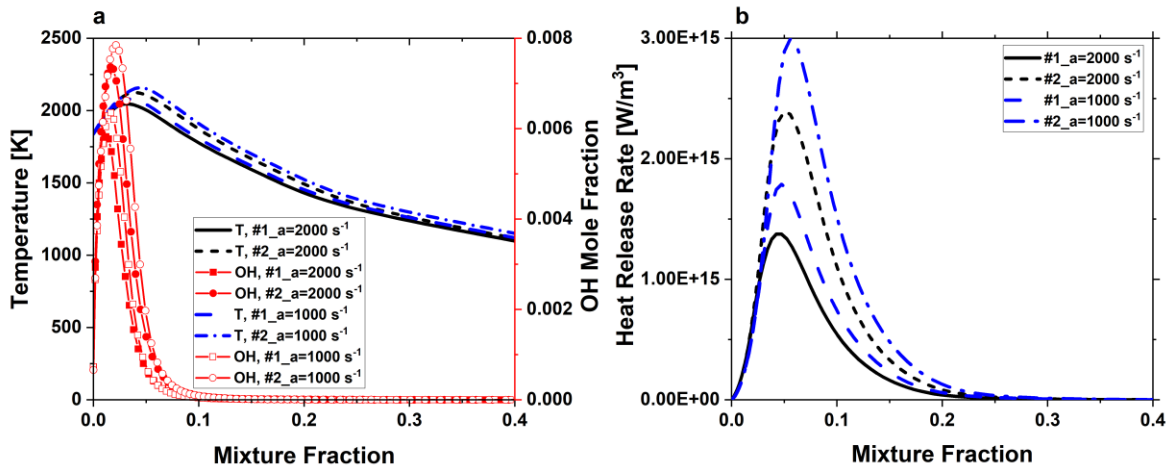

Fig. 2 1D counter flow flame COSILAB simulation results of (a) temperature, OH mole fraction, and (b) heat release rate for pure n-heptane (#1 and #2 flame conditions) at strain rates of 1000 s^{-1} and 2000 s^{-1}.

3.2 Flame appearance

Fig. 3 displays direct images of the n-heptane swirl spray flame with (QD_L) and without (QN_L) the dilution air effect, corresponding to the global equivalence ratios given in Table 2. Prior to the introduction of air dilution, yellow was the dominant color appearance in the flame, indicating the presence of soot. Two clear flame branches at the inner recirculation zone (inner flame branch, IFB) and near the outer shear layer (outer flame branch, OFB) were shown in the flame. The IFB of the QN_L flame exhibited less reaction (less luminous flame area) than the IFB of the QD_L flame. This possibly occurs because the hot product entering the IRZ is more with the effect of dilution air, making this flame branch look bigger. Introducing dilution air to the flame removed almost all the yellow luminosities. In addition, the flame was contained above the edge of the bluff-body within the outer shear layer and the height of the flame remained almost unchanged. The lift-off from the bluff-body is unclear from the direct images shown in Fig. 3.

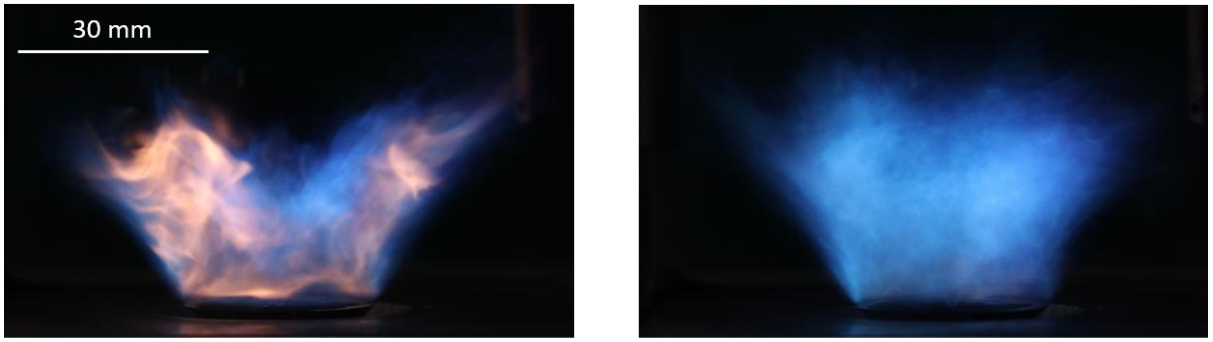

QN_L QD_L

Fig. 3, From left: n-heptane swirl spray flame without (QN_L, ϕ = 0.167) and with (QD_L, ϕ = 0.162) dilution air effect.

3.3 Stability limit testing

Stability limit testing was performed at two fuel mass flow rates: 630 g/h and 700 g/h. The blow-off condition at each fuel mass flow rate was determined first, after which dilution air was introduced. Dilution air mass flow rates were added to each case by 2% and 5% of the co-flow air mass flow rate at the blow-off conditions. For example, 2% dilution air means that the co-flow air was maintained at the blow-off condition (i.e., 790 SLPM for the condition at 630 g/h), and an additional 15.8 SLPM (2% of the 790 SLPM) was introduced through the air dilution holes. Overall, the introduction of dilution air was found to increase the stability limit. In the no-dilution case, the flame quenched at 790 SLPM (Blow-off condition). The addition of 2% dilution air allowed the flame to persist longer, with the unstable flame extinguishing after approximately 5 minutes. Whereas the introduction of 5% dilution air completely stabilized the flame, indicating the effectiveness of the dilution air strategy in enhancing the stability of bluff-body swirl flames.

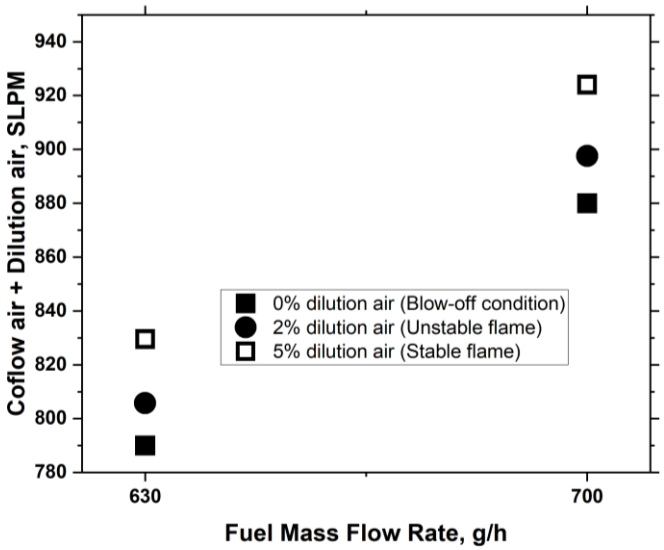

342

343 **Fig. 4** Fuel mass flow rate against the sum of co-flow air and dilution air.

344

345 ## 3.4 PIV

346 The cold flow 2D mean velocity, obtained from PIV measurements with and without dilution
347 air for the SN_H, SD1_H, and SD3_H conditions (shown in Fig. 5, left), provides insight into
348 the impact of the dilution air strategy on the flame's flow structure. The general structure of the
349 bluff-body swirl flame consists of two recirculation zones (inner and outer) and two shear
350 layers along the annular air jet flow. As presented in Fig.5 (left), for all conditions, the highest
351 velocities, as expected, are observed within the annular air jet flow, along the inner and outer
352 shear layers. The inner shear layer (ISL) separates the IRZ from the annular air jet flow, and
353 the outer shear layer (OSL) separates the ORZ from the annular air jet flow. In the common
354 bluff-body swirl flame configuration (i.e., without dilution air), recirculation zones are
355 generated by the swirling flow nature and the existence of the bluff-body, which generally
356 enhances the entrainment of gases as well as blow-off limits [31,32]. The high level of swirling
357 flow forms steep pressure gradients, which leads to vortex breakdown, resulting in the
358 formation of a large IRZ [33]. The vortices, shown in all conditions, establish a low-velocity
359 region at the center of their core, as expected. In the SN_H case shown in Fig. 5 (left), the
360 vortex created within the IRZ is located at the top of the annular jet flow (at x axis of -35 mm).

As the dilution air is introduced, the vortex starts moving downwards and inwards, towards the centre of the IRZ (at x axis of -25 mm in the SD1_H case, and at x axis of -15 mm in the SD2_H case). The location of the vortex in the SD3_H case remained almost unchanged from the SD2_H case. The addition of 2% dilution air (SD1_H) showed no significant impact on the flow structure within the flame. The addition of dilution air increased the velocity and the turbulent kinetic energy in the IRZ, as shown in Fig. 5. The movement of the vortex downwards and inwards, towards the centre of the IRZ, enhances the flame's ability to stay anchored to the bottom surface of the burner, thereby improving its overall stability. Furthermore, the increased turbulent kinetic energy and the steeper velocity gradient within the IRZ suggest enhanced recirculation and more effective fuel-air mixing (in the case of a reacting flow).

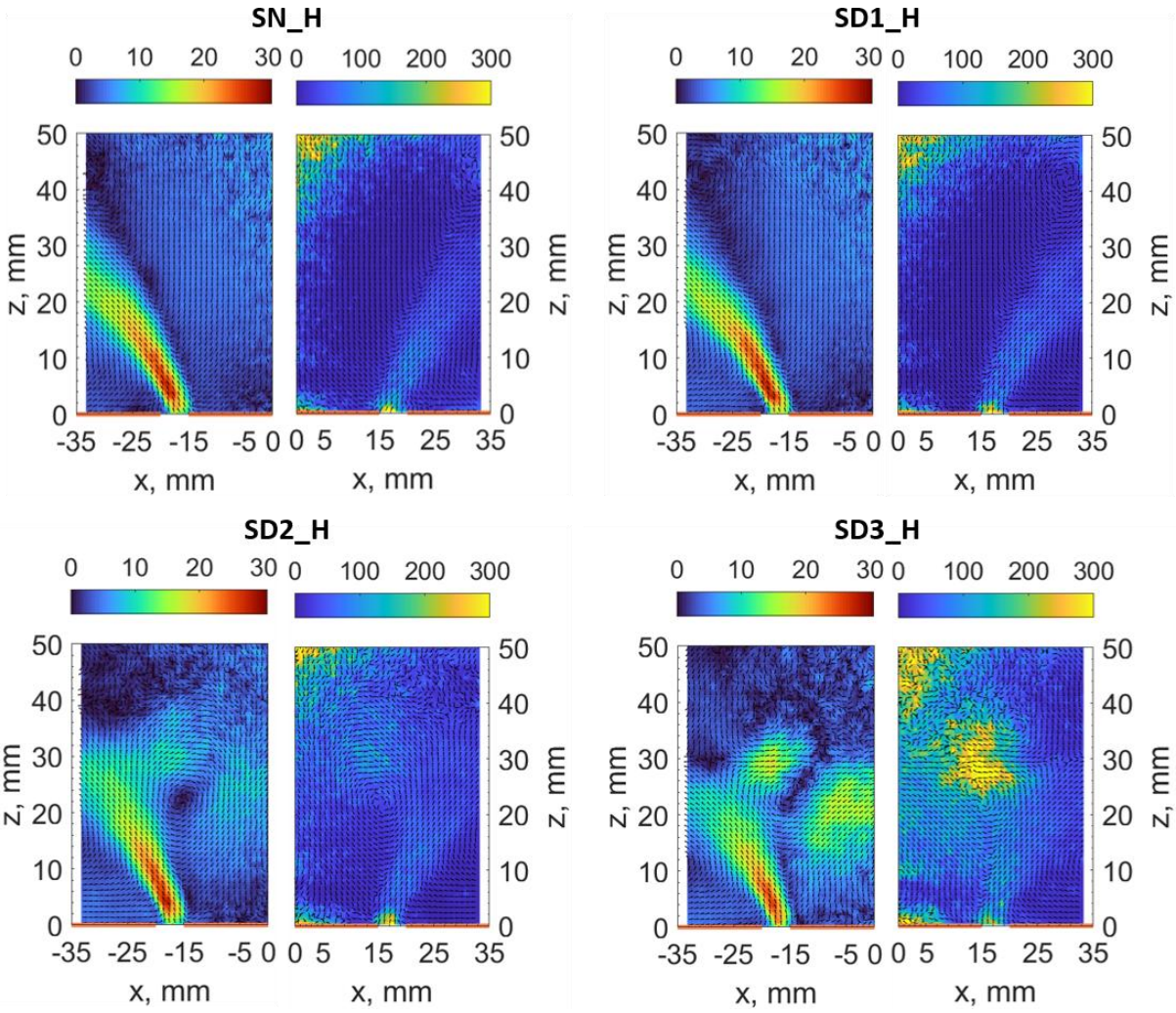

Fig. 5 cold flow contour plots of the 2D mean velocities (left) and turbulent kinetic energy (right) under stable conditions for different dilution levels: 0% (SN_H), 2% (SD1_H), 5% (SD2_H), and 10% (SD3_H). The bottom surface of the combustion chamber is highlighted in red.

Figure 6 shows the relative and cumulative energy spectra of the PIV POD modes for the SN_H, SD1_H, SD2_H, and SD3_H conditions. The relative energy of mode 1 is lower with the added dilution air conditions, as shown in Fig. 6 (a). The PIV results, in Fig. 5, showed that the addition of dilution air increases the turbulent kinetic energy, which explains the decrease in the energy percentage associated with the first mode for the SD3_H condition in Fig. 6 (a). This is because the energy is distributed across higher modes that represent smaller coherent structures, such as vortices. The cumulative energy of POD modes, shown in Fig. 6 (b), indicates the total turbulent kinetic energy captured when combining the successive modes.

Fig. 6 (b) suggests that fewer POD modes are required to capture 50% of the total turbulent kinetic energy in the no dilution condition (i.e., SN_H). This is because large coherent structures dominate the flow. Whereas in the added dilution air conditions the flow structure becomes more fragmented and so the energy is distributed across smaller-scale flow structures, requiring more modes to capture 50% of the total turbulent kinetic energy, as shown in Fig. 6 (b).

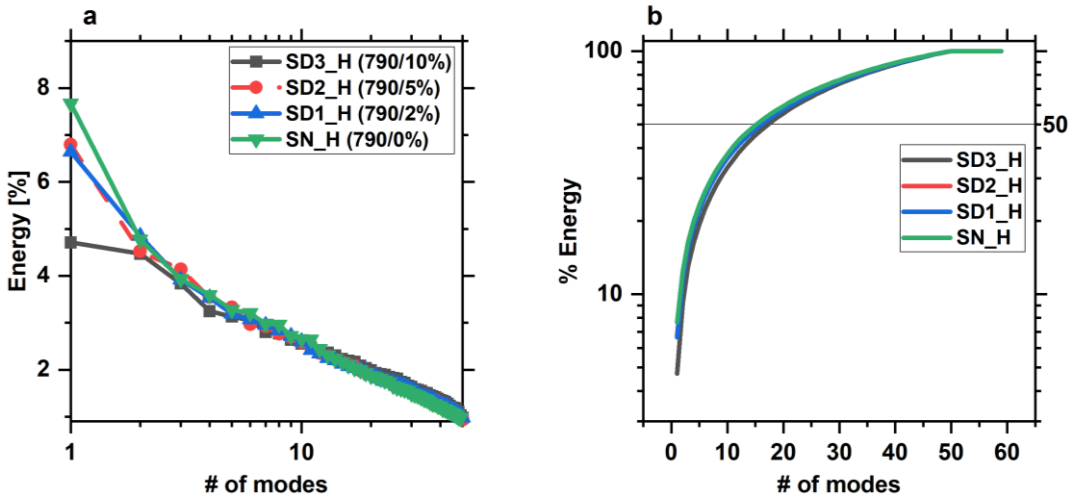

Fig. 6 relative energy of the PIV POD modes (a) and cumulative energy of the PIV POD modes (b) for the SN_H, SD1_H, SD2_H, and SD3_H conditions.

3.5 Chemiluminescence

OH* Chemiluminescence is well known as a heat release indicator. Fig. 7 displays averaged inverse Abel transformed OH* Chemiluminescence images for QN_L, QD_L, NN_L, ND_L, SN_L, and SD_L cases. The two flame branches (IFB & OFB) are shown clearly in Fig. 7 in the flame cases with no air dilution (QN_L, NN_L, and SN_L). Similar to what was observed earlier in the OH-PLIF results, OH* Chemiluminescence also confirms that the addition of dilution air confines the OFB further toward the center of the flame due to the high air strain caused by the air dilution. At all three flow conditions, the addition of dilution air increased the OH* signal (i.e., heat release rate) by 148%, 128%, and 47% for blow-off, near blow-off, and stable conditions, respectively, compared with the counterparts without dilution. This increase

404 is because of the rapid mixing between air and fuel, hence more recirculation of hot combustion
405 products inside the IRZ. The results presented in Fig. 7 show that the inner recirculation zone
406 is where the OH* signals are at their greatest. More details on the flow field motion can be
407 observed from a PIV study in the future. The addition of dilution air by 2% of the air co-flow
408 (i.e., SD1_H) did not cause any increase in the HRR, as shown in Fig. 7. Whereas adding
409 dilution air by 5% and 10% (i.e., SD2_H & SD3_H) of the air co-flow increased the heat release
410 rate by about 132% and 247%, respectively.

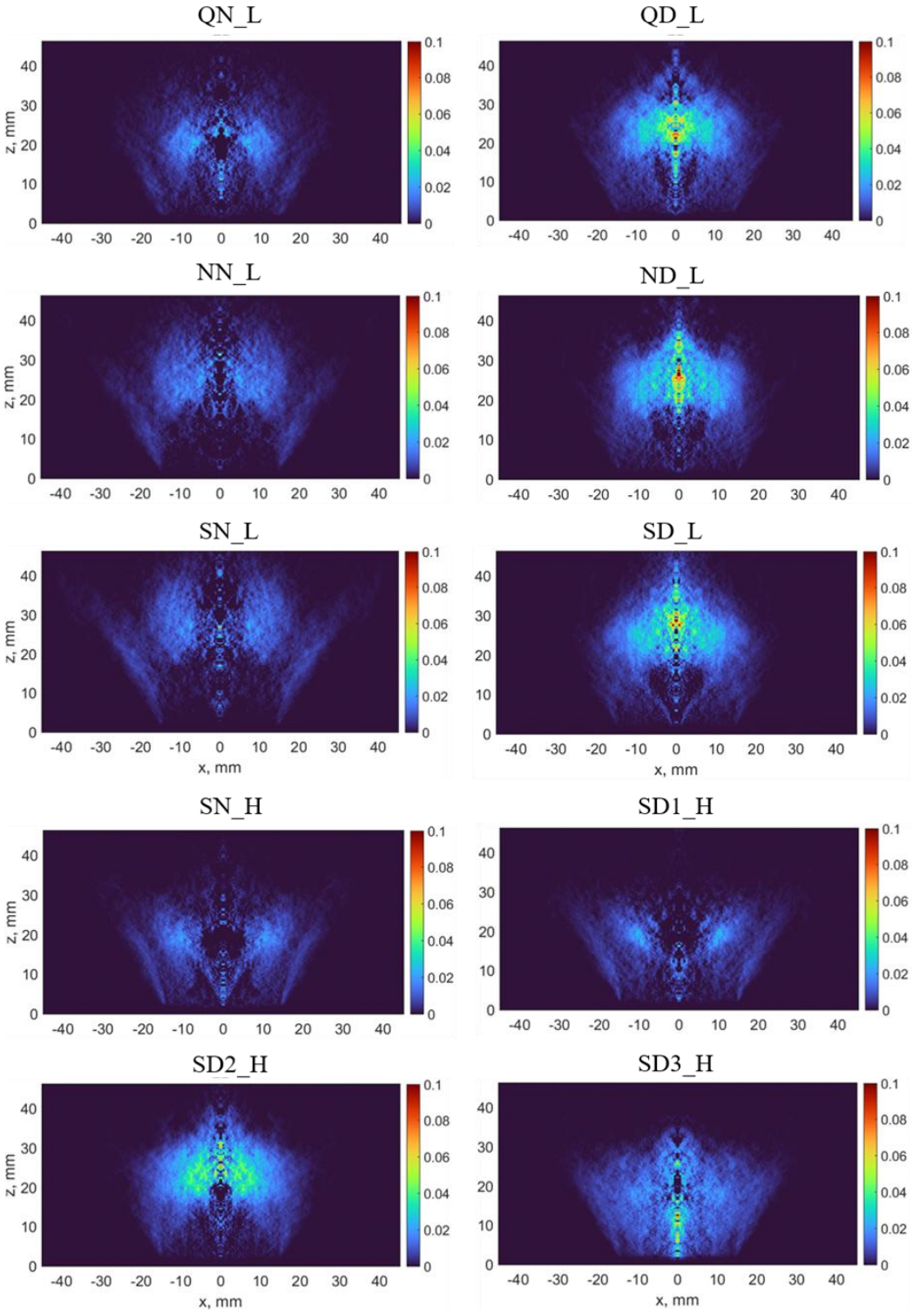

Fig. 7 Averaged inverse Abel transformed images of OH* Chemiluminescence for QN_L, QD_L, NN_L, ND_L, SN_L, SD_L SN_H, SD1_H, SD2_H, and SD3_H cases.

3.6 PLIF

3.6.1 Fuel-PLIF

The background B(Q) signal near the Q1(6) transition was used to correct the background noise and to study the impact of dilution air on the fuel fluorescence signal, including the fuel trajectory and spray droplets. Fig. 8 presents the mean images of the fuel-PLIF signal for the SN_H, SD1_H, SD2_H, and SD3_H. The overall spray trajectory and structure of all the cases have a cone-like shape. However, the droplet dispersion differs significantly. The effect of adding dilution air was found to break up the liquid fuel jet into more droplets and spread them more broadly towards the IRZ region. This is caused by the force exerted (such as the aerodynamic drag force) from the diluted air combined with the recirculation air hitting the droplets. This enhances the direct removal of small droplets from the liquid jets surface (shear breakup). The surface area covered by the droplets increases with the increase of the amount of very small droplets, and hence the heat and mass exchange rates increase too. Therefore, the radial injection of air dilution produces fast mixing and a more stable flame.

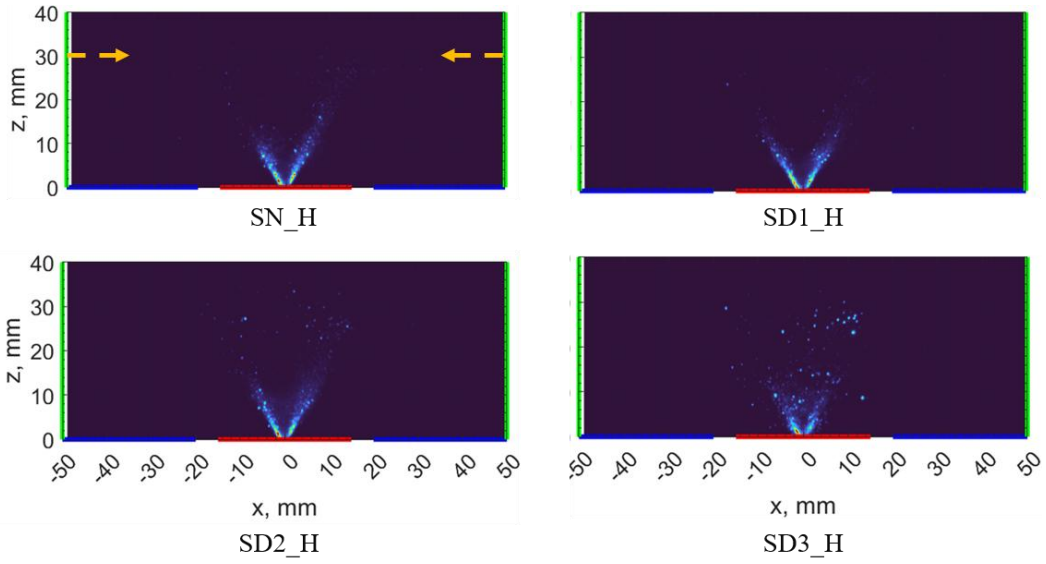

Fig. 8 Mean images of fuel-PLIF signal for SN_H, SD1_H, SD2_H, and SD3_H. The arrows shown in the SN_H case indicate the height of dilution air injection (this applies to all cases).

3.6.2 OH-PLIF

In this study, the OH-PLIF images are used to give information and insight on the flame sheet characteristics affected by the introduction of dilution air. Fig. 9 shows the instantaneous and averaged images of OH-PLIF for QN_L, QD_L, NN_L, ND_L, SN_L, and SD_L. The instantaneous images suggest that cases without the dilution air (i.e., QN_L, NN_L, and SN_L) mostly have continuous OH flame sheets, in which the flame sheet in the OFB is extended from one edge of the bluff-body to the other edge. The flame sheet in the cases with dilution air (i.e., QD_L, ND_L, and SD_L) presents more local extinction due to the high turbulence level. The relatively small mass fuel flow rates used in this study (630 g/h and 700 g/h) resulted in a low effective liquid atomization, in which droplets were not efficiently broken to the finest size. This resulted in fuel-LIF signals from the fuel droplets contained in the OH-PLIF results, such as the signals found along the spray V-shape trajectory, adding difficulty in analyzing the characteristics of IRZ. The instantaneous images in Fig. 9 clearly show the fuel-LIF signal. With background correction, the averaged images in Fig. 9 mostly show no signal where the spray V-shape trajectory occurs. Nevertheless, few fuel-PLIF signals remain in the averaged OH-PLIF, as seen clearly in the QN_L case in Fig. 9. Therefore, for a better comparison, relative OH intensity data across the height of 10 mm (Z-axis) were extracted and plotted against the radial position, see Fig. 11, to avoid interference with the fuel-PLIF signal.

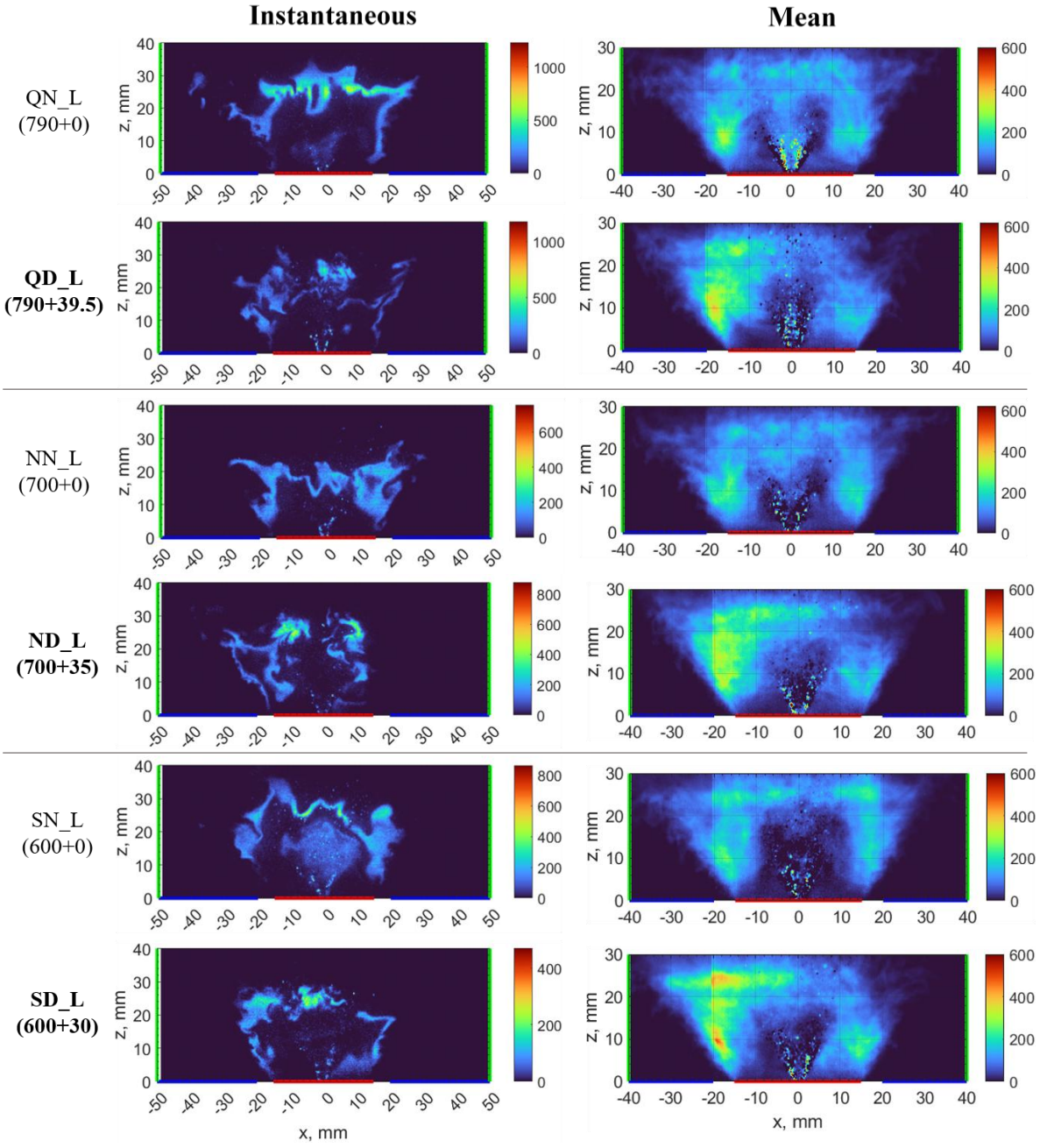

Fig. 9 Instantaneous and averaged images of OH-PLIF for QN_L, QD_L, NN_L, ND_L, SN_L, and SD_L. Bracketed numbers underneath the case names denote the annular air flow rate (SLPM) + dilution air flow rate (SLPM). The laser beam's location is shown in green, the combustion chamber's bottom surface is shown in blue, and the surface of the bluff body is shown in red.

Figure 10 displays the instantaneous and averaged images of OH-PLIF for QN_H, QD_H, SN_H, SD1_H, SD2_H, and SD3_H. The observations presented here are similar to those delivered by Fig. 9 regarding the direct relationship between the local extinction and dilution air. Nevertheless, it is shown in Fig. 10 that the addition of dilution by 2% (SD1_H) of the co-flow air did not have a big impact on the flame sheet continuity, but it only shrank towards the

center of the flame and bluff-body. The corrected averaged OH-PLIF images suggest that adding dilution air increases the relative OH intensity in the OFB. This can be noticed by the increase in the red and yellow colour in the mean images (Fig. 10) on adding more dilution air.

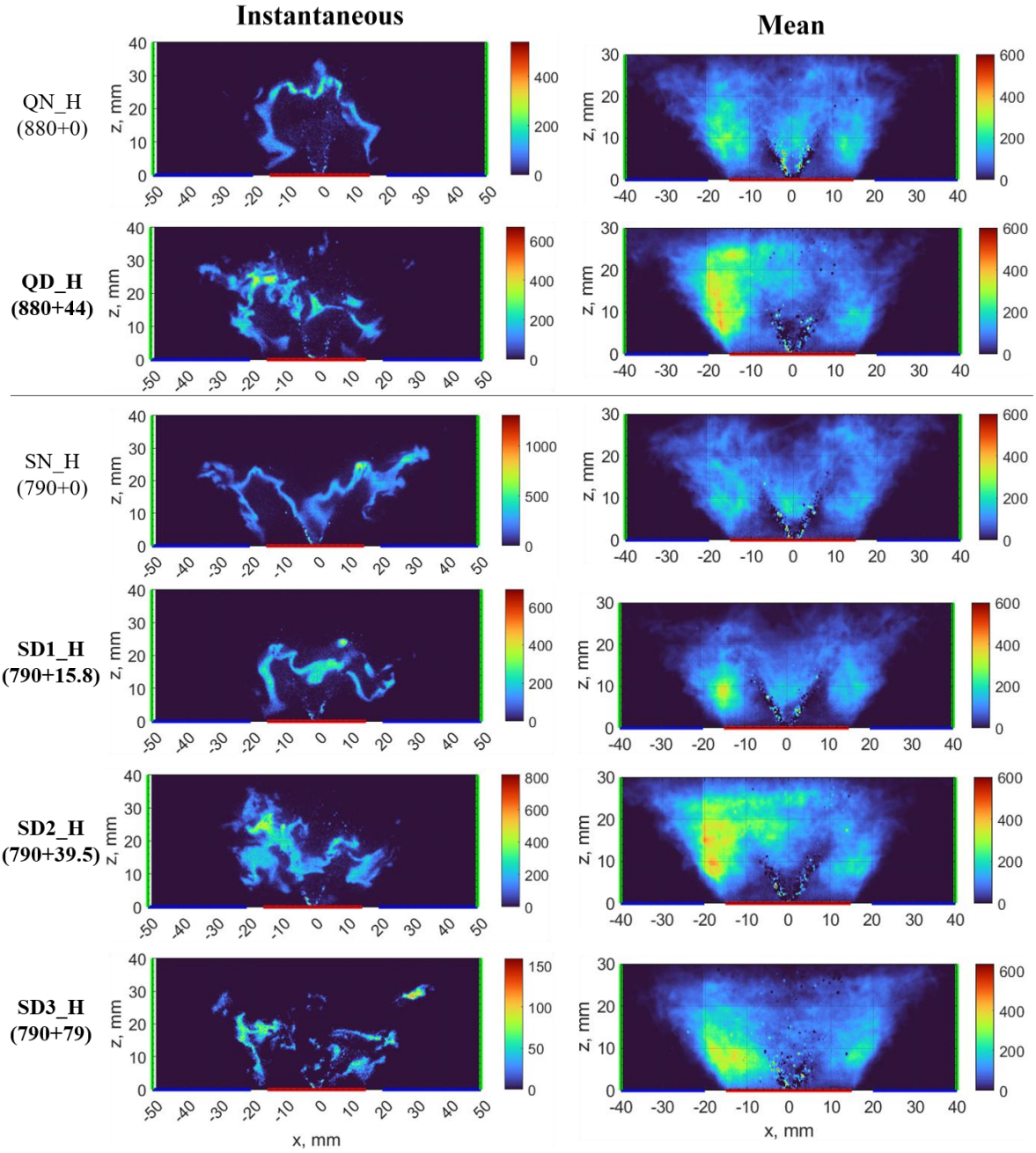

Fig. 10 Instantaneous and averaged images of OH-PLIF for QN_H, QD_H, SN_H, SD1_H, SD2_H, and SD3_H. Bracketed numbers underneath the case names denote the annular air flow rate (SLPM) + dilution air flow rate (SLPM). The laser beam's location is shown in green, the combustion chamber's bottom surface is shown in blue, and the surface of the bluff body is shown in red.

The relative OH intensity across the height of 10 mm in the Z-axis was plotted against the radial position for all cases in Fig. 11. In cases where air dilution was added, the relative

intensity of OH was higher and the location where the OH peak values occur is reasonably consistent in all cases. The OFB is where the OH intensity peaks above the region where the annular air enters the chamber. The IRZ is found to have lower OH intensities generally than OFB. Without dilution air addition, the blow-off condition had higher OH intensity than the stable condition. However, adding dilution air to both conditions (stable and blow-off) increased the OH intensity to higher levels for the stable conditions compared to the blow-off case. Measurements shown in Fig. 11 are plotted at 10 mm above the nozzle, so the peak values shown do not necessarily correspond to the peak values of the overall OH because the flame may become more compact when approaching the bluff-body in the blow-off condition. The cases with dilution air (dashed lines in Fig. 11) have higher OH signal than those without dilution air (solid lines in Fig. 11) at the same conditions. This means that the flame heights are similar at the same conditions, and therefore the OFB has a higher OH signal in cases with dilution air.

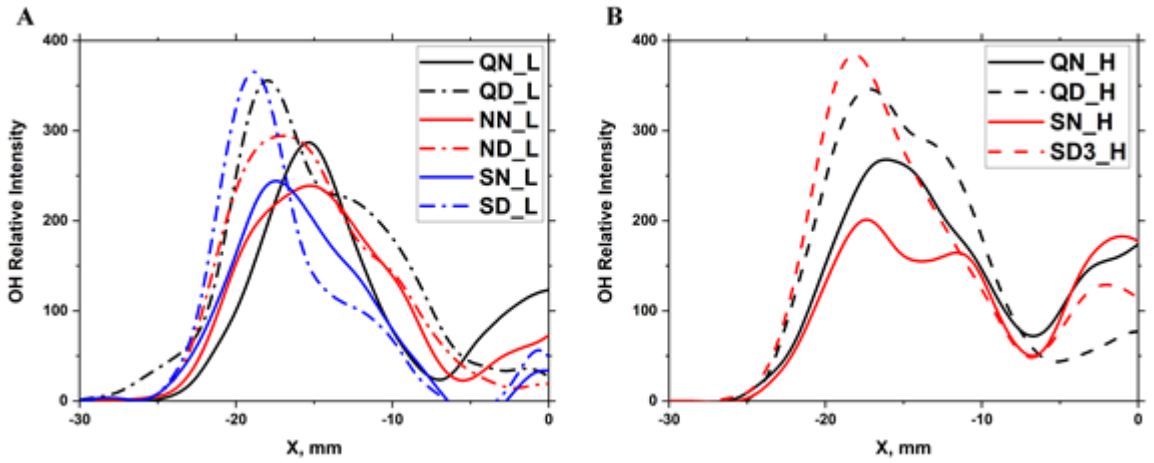

Fig. 11 Relative OH intensity across the height of 10 mm in the Z-axis against the radial position for (A) cases with fuel mass flow rate of 630 g/h, and (B) cases with fuel mass flow rate of 700 g/h.

3.6.3 Local extinction & lift-off

Local extinction and lift-off characteristics of the flame sheets were investigated through the OH-PLIF results. Fig. 12 illustrates the PDF against the number of local extinction events for

all cases. Generally, all cases with dilution air added exhibited higher PDF of local extinction events than those without dilution air. The addition of dilution air (5% of air co-flow) to the cases with a lower fuel mass flow rate of 630 g/h resulted in increasing the occurrence of local extinction by 6-7.5%, regardless of the flame condition (i.e., at quenching, near blow-off, or stable condition). Whereas adding dilution air (5% of air co-flow) to the cases with a higher fuel mass flow rate of 700 g/h increased the occurrence of local extinction by 3.9%. The addition of dilution air by 2% of the air co-flow (i.e. SD1_H case) had a negligible impact on the amount of local extinction occurrence. These percentages are calculated based on the difference of the areas under the curves.

The increase in the degree of local extinction with the addition of dilution air is due to the high turbulence flow. Local extinction occurrences were likely caused by the air strain that the high turbulence levels put on the flame front. The rate of diffusive mixing is accelerated by turbulence, which raises the flame surface area and scalar gradients [34]. Rapid mixing makes higher HRR possible. Nevertheless, the rise in mixing rates could result in quenching the flame. The current cases studied in this work showed more stability when more dilution air was added to the flame despite the fact that local extinction events also increased. This could mean that the rates of heat diffusion did not outpace the rate of combustion's heat release in the current cases.

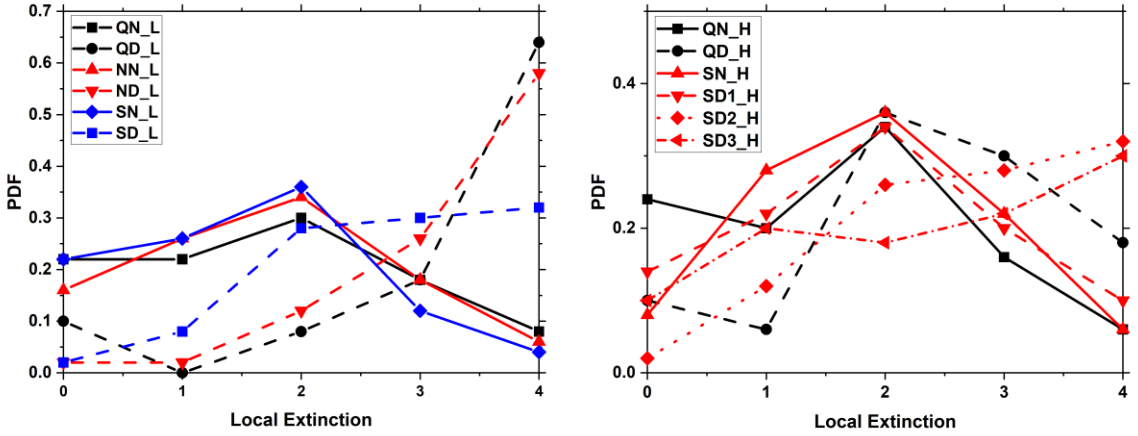

Fig. 12 PDF of local extinction of (left) cases with fuel mass flow rate of 630 g/h, and (right) cases with fuel mass flow rate of 700 g/h.

Figure 13 shows the PDF of the lift-off height for all cases. The lift-off height decreased on moving from the stable condition towards the blow-off condition. Overall, the mean lift-off height reduces only slightly with the addition of dilution air. The addition of dilution air (5% of air co-flow) decreased the mean lift-off heights by about 0.007-0.01%. The lift-off heights were reduced by roughly 0.0145% when dilution air (10% of the air co-flow) was added. Therefore, there is almost no impact of the dilution air on the lift-off heights at the flow conditions tested.

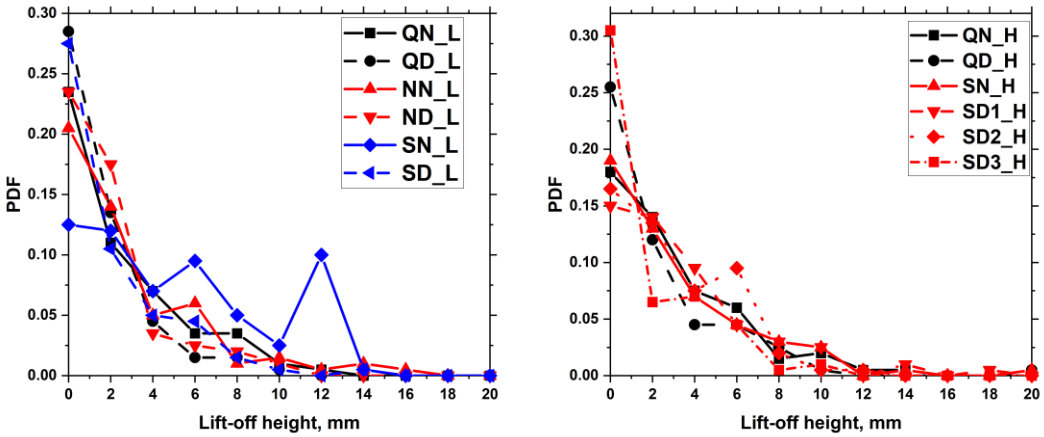

Fig. 13 PDF of lift-off height of (left) cases with fuel mass flow rate of 630 g/h, and (right) cases with fuel mass flow rate of 700 g/h.

4. Conclusion

This work primarily focuses on the impact of the dilution air introduction on flame structure and flame stability including local extinction and lift-off of the n-heptane bluff-body swirl spray flame. Multiple flow conditions, with and without dilution air, at global blow-off, near blow-off, and stable conditions have been studied and compared in this study. Preliminary understanding on the impact of the flame structure behaviour and temperature when adding more air with hot products has been conducted through 1D non-premixed laminar counter flow flame simulations. In addition, experimental studies have been carried out in which fuel-PLIF and OH-PLIF measurements were collected to analyse the impact of dilution air introduction on fuel spray atomization, flame structure, and stability.

Based on the experimental and numerical results, the key conclusions of this study as follows:

- The 1D simulations showed that 10% addition of more air on the oxidiser side increased the peak value of the temperature by approximately 3.9%, along with corresponding increases in the HRR and OH mole fraction.
- Direct imaging showed that the addition of dilution air removed most of the yellow luminosity associated with soot. In addition, the flame branch in the IRZ expanded to cover a larger area in the case with added dilution air.
- The flame stability limits improved with dilution air; adding 5% dilution air stabilized the flame completely under conditions where the non-diluted flame blew off.
- More efficient spray breakup near the nozzle region detected with the addition of dilution air.
- OH flame sheets in the cases without dilution air were mostly continuous and thin compared to the diluted cases where flame sheets appeared more cloud-shaped and wrinkled. Statistical analysis of the OH-PLIF results showed that adding 5% dilution

555 air increased local extinction events by up to 7.5%, primarily due to the intense
556 aerodynamic strain imposed on the flame front under highly turbulent conditions.
557 • OH* chemiluminescence measurements indicated negligible change in heat release rate
558 with 2% dilution air, while increases of approximately 132% and 247% were observed
559 with 5% and 10% dilution, respectively.

560 Overall, the addition of dilution air was also found to enhance the stability of the flame,
561 which increases the flexibility for gas turbine engines to operate under leaner conditions,
562 improving combustion efficiency, and thus local operational cost, and lower emissions.

563

564 ## Acknowledgements

565 The authors would like to acknowledge EPSRC for the funding support of the research projects
566 [Grant Refs: EP/S017259/2 and EP/Y020839/1]. For the purpose of open access, the author
567 has applied a 'Creative Commons Attribution (CC BY) licence to any Author Accepted
568 Manuscript version arising.

569

570 ## References

571 [1] P. Flohr, P. Stuttaford, Combustors in gas turbine systems, Mod. Gas Turbine Syst.
572 High Effic. Low Emiss. Fuel Flex. Power Gener. (2013) 151-191e.
573 https://doi.org/10.1533/9780857096067.2.151.

574 [2] D.C. Dayton, T.D. Foust, Optimized Biofuels for High-Efficiency, Low-Emission
575 Engines, Anal. Methods Biomass Charact. Convers. (2020) 129–145.
576 https://doi.org/10.1016/B978-0-12-815605-6.00009-3.

577 [3] N. Syred, J.M. Beér, Combustion in swirling flows: A review, Combust. Flame. 23
578 (1974) 143–201. https://doi.org/10.1016/0010-2180(74)90057-1.

[4] S. Candel, D. Durox, T. Schuller, J.F. Bourgouin, J.P. Moeck, Dynamics of swirling flames, Annu. Rev. Fluid Mech. 46 (2014) 147–173. https://doi.org/10.1146/annurev-fluid-010313-141300.

[5] R.M. Pierce, S.A. Mosier, C.E. Smith, B.S. Hinton, Advanced combustion systems for stationary gas turbine engines. Volume II. Bench scale evaluation. Final report September 1976-January 1978, (1980).

[6] I. El Helou, J.M. Foale, R.S. Pathania, R. Ciardiello, A.W. Skiba, A comparison between fossil and synthetic kerosene flames from the perspective of soot emissions in a swirl spray RQL burner, Fuel. 331 (2023) 125608. https://doi.org/10.1016/j.fuel.2022.125608.

[7] H. Liu, Q. Tang, Z. Yang, X. Ran, C. Geng, B. Chen, L. Feng, M. Yao, A comparative study on partially premixed combustion (PPC) and reactivity controlled compression ignition (RCCI) in an optical engine, Proc. Combust. Inst. 37 (2019) 4759–4766. https://doi.org/10.1016/j.proci.2018.06.004.

[8] H. Liu, Y. Cui, M. Wen, Z. Ming, C. Jin, L. Feng, R. Tang, S. Cheng, Optical diagnostics and chemical kinetic analysis on partially premixed combustion characteristics fueled with methanol and various cetane improvers, Proc. Combust. Inst. 40 (2024) 105214. https://doi.org/10.1016/j.proci.2024.105214.

[9] A. Giusti, E. Mastorakos, Turbulent Combustion Modelling and Experiments: Recent Trends and Developments, Flow, Turbul. Combust. 103 (2019) 847–869. https://doi.org/10.1007/S10494-019-00072-6/FIGURES/4.

[10] Q. Wang, Z. Chen, J. Wang, L. Zeng, X. Zhang, X. Li, Z. Li, Effects of secondary air distribution in primary combustion zone on combustion and NOx emissions of a large-scale down-fired boiler with air staging, Energy. 165 (2018) 399–410.

https://doi.org/10.1016/j.energy.2018.09.194.

[11] K. Kikuchi, R. Murai, T. Hori, F. Akamatsu, Fundamental study on ammonia low-NOx combustion using two-stage combustion by parallel air jets, Processes. 10 (2022). https://doi.org/10.3390/pr10010023.

[12] U. Trivanovic, S.E. Pratsinis, Trade-off between soot and NO emissions during enclosed spray combustion of jet fuel, Sci. Rep. 14 (2024) 1–11. https://doi.org/10.1038/s41598-024-73484-8.

[13] I. El Helou, A.W. Skiba, E. Mastorakos, Experimental Investigation of Soot Production and Oxidation in a Lab-Scale Rich–Quench–Lean (RQL) Burner, Flow, Turbul. Combust. 106 (2021) 1019–1041. https://doi.org/10.1007/S10494-020-00113-5/FIGURES/11.

[14] G. De Falco, I. El Helou, P.M. de Oliveira, M. Sirignano, R. Yuan, A. D'Anna, E. Mastorakos, Soot particle size distribution measurements in a turbulent ethylene swirl flame, Proc. Combust. Inst. 38 (2021) 2691–2699. https://doi.org/10.1016/J.PROCI.2020.06.212.

[15] K.P. Geigle, W. Meier, R. Hadef, Soot formation and flame characterization of an aero-engine model combustor burning ethylene at elevated pressure, Proc. ASME Turbo Expo. 1 B (2013) 1–8. https://doi.org/10.1115/GT2013-95316.

[16] K.P. Geigle, W. O'Loughlin, R. Hadef, W. Meier, Visualization of soot inception in turbulent pressurized flames by simultaneous measurement of laser-induced fluorescence of polycyclic aromatic hydrocarbons and laser-induced incandescence, and correlation to OH distributions, Appl. Phys. B Lasers Opt. 119 (2015) 717–730. https://doi.org/10.1007/S00340-015-6075-3/FIGURES/11.

626 [17] M. Stöhr, K.P. Geigle, R. Hadef, I. Boxx, C.D. Carter, M. Grader, P. Gerlinger, Time-
627 resolved study of transient soot formation in an aero-engine model combustor at
628 elevated pressure, Proc. Combust. Inst. 37 (2019) 5421–5428.
629 https://doi.org/10.1016/J.PROCI.2018.05.122.

630 [18] T.M. Farag, M. Arai, M. Shimizu, H. Hiroyasu, The Effect of Fuel Volatility on Spray
631 Flame Stabilization, Bull. JSME. 26 (1983) 1753–1760.
632 https://doi.org/10.1299/JSME1958.26.1753.

633 [19] R. Yuan, J. Kariuki, E. Mastorakos, Measurements in swirling spray flames at blow-
634 off, Orig. Res. Artic. (n.d.). https://doi.org/10.1177/1756827718763559.

635 [20] D.E. Cavaliere, J. Kariuki, E. Mastorakos, A Comparison of the Blow-Off Behaviour
636 of Swirl-Stabilized Premixed, Non-Premixed and Spray Flames, Flow Turbul.
637 Combust. 91 (2013) 347–372. https://doi.org/10.1007/s10494-013-9470-z.

638 [21] R.S. Pathania, I. El Helou, A.W. Skiba, R. Ciardiello, E. Mastorakos, Lean blow-off of
639 premixed swirl-stabilised flames with vapourised kerosene, Proc. Combust. Inst. 39
640 (2023) 2229–2238. https://doi.org/10.1016/j.proci.2022.10.006.

641 [22] C. Zhang, P. Zou, B. Wang, X. Xue, Y. Lin, C. Sung, COMPARISON OF FLAME
642 DYNAMICS AT STABLE AND NEAR-LBO CONDITIONS FOR SWIRL-
643 STABILIZED KEROSENE SPRAY COMBUSTION, Proc. ASME Turbo Expo 2015
644 Turbine Tech. Conf. Expo. (2015) 1–10.

645 [23] Chemical Mechanism: Combustion Research Group at UC San Diego, (n.d.).
646 https://web.eng.ucsd.edu/mae/groups/combustion/mechanism.html (accessed
647 September 7, 2021).

648 [24] COSILAB, 1-D and Counterflow Flames, (2018).

649 [25] J.A.M. Sidey, E. Mastorakos, Simulations of laminar non-premixed flames of methane
650 with hot combustion products as oxidiser, Combust. Flame. 163 (2016) 1–11.
651 https://doi.org/10.1016/j.combustflame.2015.07.034.

652 [26] A.A. Saleh, K.J. Hughes, R. Yuan, Reaction zone characteristics of iso-pentanol swirl
653 spray flames using OH-PLIF and 2C-LII, Proc. Combust. Inst. 39 (2023) 2663–2672.
654 https://doi.org/10.1016/J.PROCI.2022.07.232.

655 [27] A. Abu Saleh, T. Knight, R. Yuan, Application of Planar Time-Resolved 2C-LII for
656 Soot Emission Measurements in Diffusion Flames of DME Blends and in Swirl Spray
657 Flames, AIAA SCITECH 2022 Forum. (2022). https://doi.org/10.2514/6.2022-1942.

658 [28] W. Thielicke, R. Sonntag, Particle Image Velocimetry for MATLAB: Accuracy and
659 enhanced algorithms in PIVlab, J. Open Res. Softw. 9 (2021) 1–14.
660 https://doi.org/10.5334/JORS.334.

661 [29] A.G. De Mitri, R. de L. Amaral, H.L. de Moura, J.S. Ayala, J.R. Nunhez, G.J. de
662 Castilho, Tilted PIV: A novel approach for estimating the turbulent kinetic energy in
663 stirred tanks, Meas. J. Int. Meas. Confed. 217 (2023).
664 https://doi.org/10.1016/j.measurement.2023.113112.

665 [30] P. Malbois, E. Salaün, A. Vandel, G. Godard, G. Cabot, B. Renou, A.M. Boukhalfa, F.
666 Grisch, Experimental investigation of aerodynamics and structure of a swirl-stabilized
667 kerosene spray flame with laser diagnostics, Combust. Flame. 205 (2019) 109–122.
668 https://doi.org/10.1016/j.combustflame.2019.03.041.

669 [31] A. Abu Saleh, Low-Carbon Biofuels : Optical and Numerical Analysis of Combustion
670 Performance, University of Sheffield, 2023.

671 [32] D. Feikema, R.H. Chen, J.F. Driscoll, Blowout of nonpremixed flames: Maximum

672 coaxial air velocities achievable, with and without swirl, Combust. Flame. 86 (1991)
673 347–358. https://doi.org/10.1016/0010-2180(91)90128-X.

674 [33] A. Mardani, B. Asadi, A.A. Beige, Investigation of flame structure and precessing
675 vortex core instability of a gas turbine model combustor with different swirler
676 configurations, Phys. Fluids. 34 (2022). https://doi.org/10.1063/5.0097430.

677 [34] D.O. Lignell, J.H. Chen, H.A. Schmutz, Effects of Damköhler number on flame
678 extinction and reignition in turbulent non-premixed flames using DNS, Combust.
679 Flame. 158 (2011) 949–963. https://doi.org/10.1016/j.combustflame.2010.10.027.

680